Supplementary Information (SI) for Sustainable Energy & Fuels.

Spin Polarization Porous Transport Layer for Anion Exchange Membrane Water Electrolyzers with a Current Density of 11.5 A cm^{-2}

Tae Hyung Kim,‡[a] Chuan Hu,‡[a] Hyeon Keun Cho,[a] Seung Hyun Jae,[a] Sujin Lee,[b] Bongjun Yeom,[b] Young Moo Lee*[a] and Young-Hoon Kim*[a]

[a]Department of Energy Engineering, Hanyang University, 222 Wangsimni-ro, Seongdong-gu, Seoul 04763, Republic of Korea

[b]Department of Chemical Engineering, Hanyang University, 222 Wangsimni-ro, Seongdong-gu, Seoul 04763, Republic of Korea

‡These authors contributed equally to this work.

Authors to whom correspondence should be addressed: E-mail: ymlee@hanyang.ac.kr, younghoonkim@hanyang.ac.kr

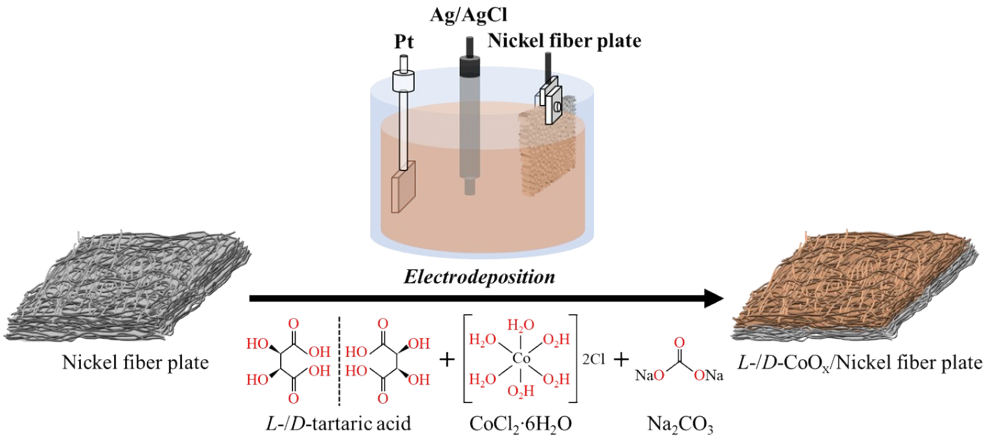

Fig. S1 Schematic diagram of direct electrodeposition of chiral amorphous CoO_x on a nickel fiber plate porous transport layer (PTL) to fabricate a spin polarization PTL (SP-PTL).

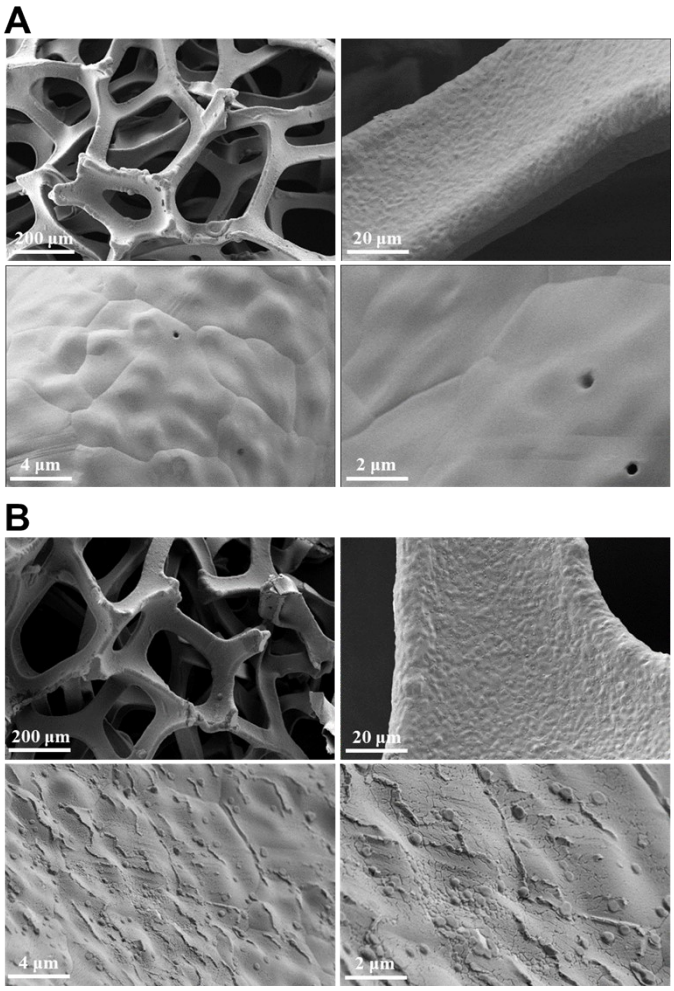

Fig. S2 SEM images of (A) pristine nickel fiber plate PTL and (B) electrodeposited *L*-CoO_x-PTL.

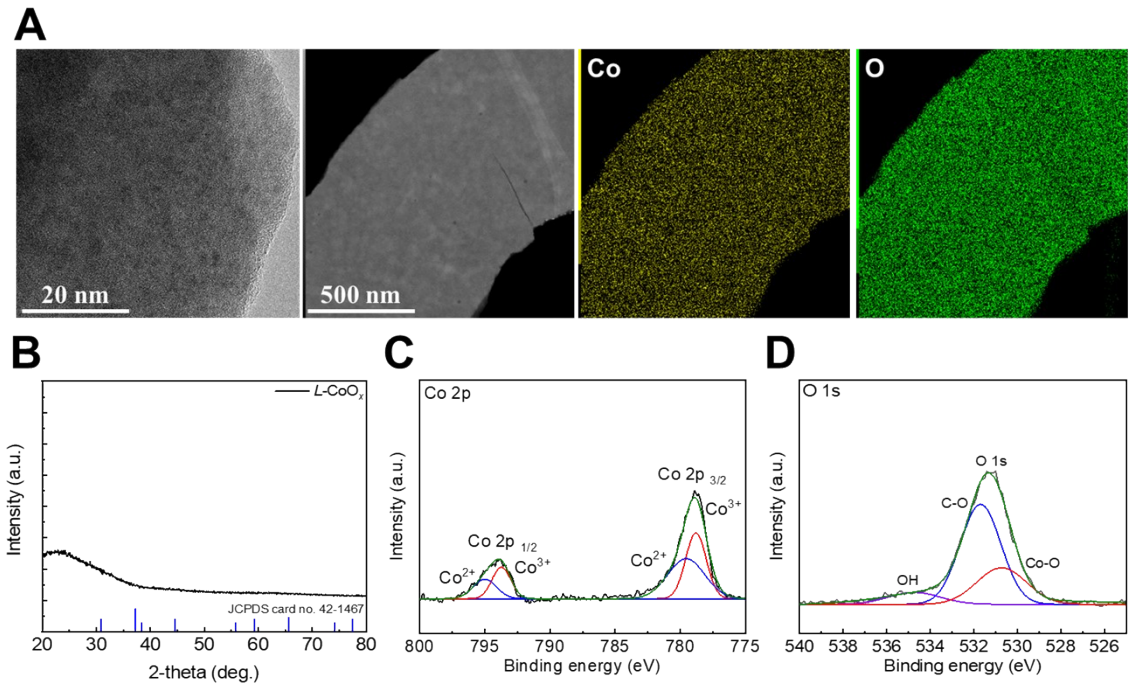

Fig. S3 (A) TEM images and elemental mapping images (Co and O) of *L*-CoO_x-spin polarization layer (SPL) thin film. (B) Grazing incidence X-ray diffraction (GIXRD) peaks of *L*-CoO_x-SPL. X-ray photoelectron spectroscopy (XPS) spectra of *L*-CoO_x-SPL thin film ((C) Co 2p peaks and (D) O 1s peaks).

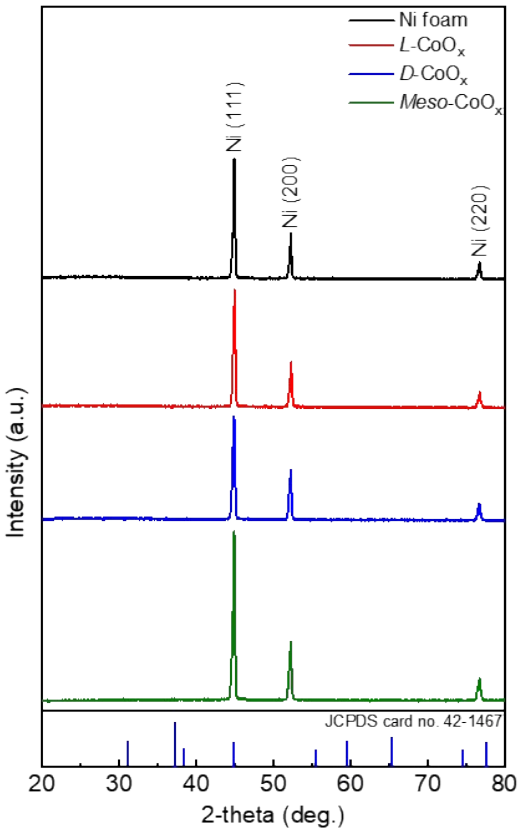

Fig. S4 XRD peaks of Ni foam, *L*-CoO_x-SPL, *D*-CoO_x-SPL and *meso*-CoO_x-layer.

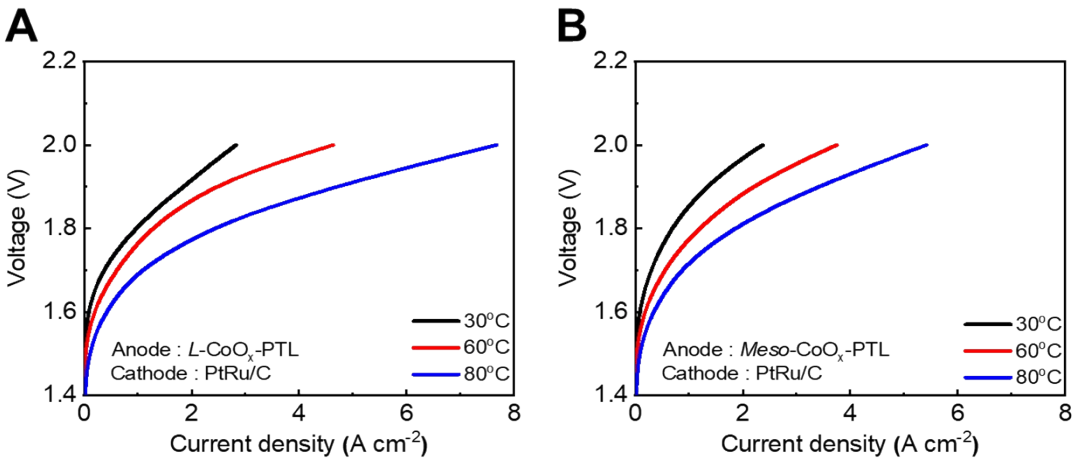

Fig. S5 Polarization curves of single-cell anion exchange membrane water electrolyzers (AEMWEs) with (A) *L*-CoO_x-PTL and (B) *meso*-CoO_x-PTL in 1 M KOH at temperatures ranging from 30℃ to 80℃.

As the temperature increased to 30℃, 60℃ and 80℃, the current density increased for both *L*-CoO_x-PTL and *meso*-CoO_x-PTL (2.83, 4.63 and 7.68 A cm^{-2} for *L*-CoO_x-PTL; 2.37, 3.75 and 5.42 cm^{-2} for *meso*-CoO_x-PTL), highlighting the significant influence of temperature on electrode kinetics.

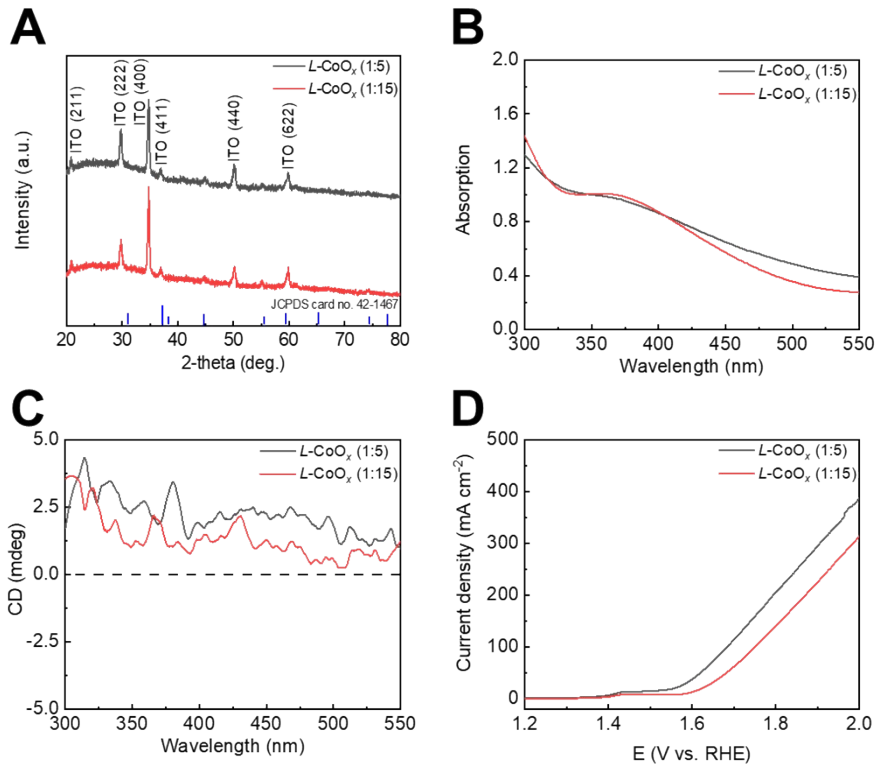

Fig. S6 (A) XRD patterns, (B) absorption spectra, (C) CD spectra and (D) LSV curves of half-cells for electrodeposited thin films prepared with varying molar ratio of $CoCl_2 \cdot 6H_2O$ to *L*-TA (1:5 and 1:15).

To optimize the deposition conditions for the *L*-CoO_x, we varied the ratios of $CoCl_2 \cdot 6H_2O$ to *L*-tartaric acid (TA) from 1:5 to 1:15 and electrodeposited the films onto ITO substrates. The resulting samples were analyzed by XRD and CD spectroscopy to examine potential structural variations (Fig. S6). Both samples did not show any sharp crystalline peaks corresponding Co_3O_4 (JCPDS card no. 42-1467) except crystalline ITO peaks (JCPDS card no. 06-0416), indicating that formed CoO_x films are amorphous (Fig. S6A). Moreover, both samples exhibited chiroptical properties similar to those obtained under the 1:10 condition, indicating that neither the crystallinity nor the chirality was significantly affected (Fig. S6B and S6C).

The overpotential at 10 mA cm-2 for both deposition conditions of 1:5 and 1:10 exhibited similar catalytic activity (314 mV for 1:5 and 313 mV for 1:10), as confirmed by the linear sweep voltammetry (LSV) curves of half-cells. However, the overpotential increased for the 1:15 ratio (352 mV) (Fig. S6D). Therefore, the 1:10 ratio was selected as the optimal deposition condition.

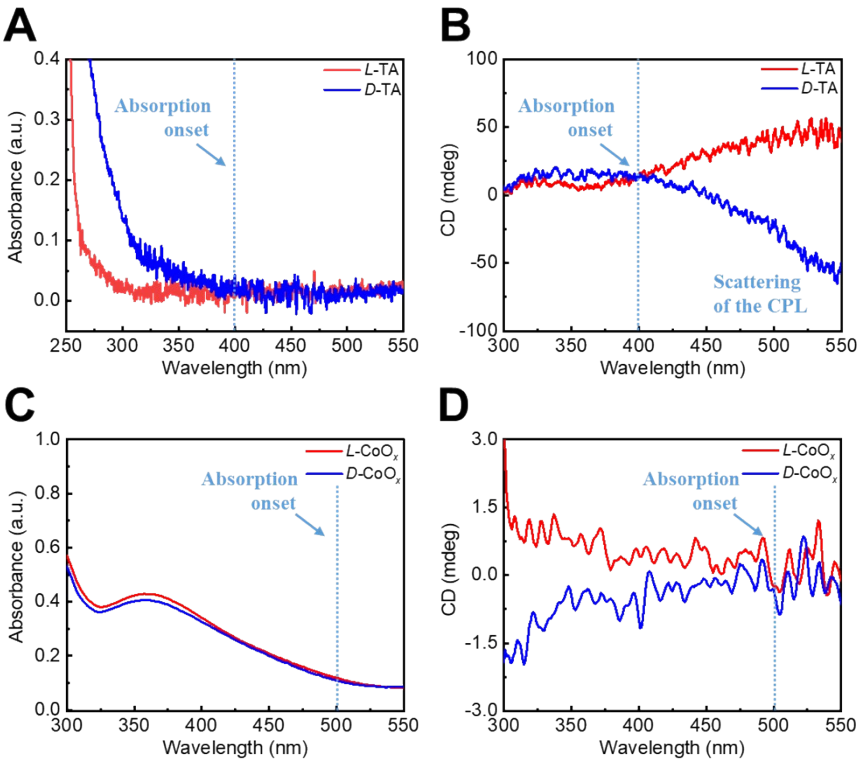

Fig. S7 Circular dichroism (A) and absorption spectra (B) of *L*-TA and *D*-TA precursor solutions and circular dichroism (C) and absorption spectra (D) of *L*-CoO_x-SPL and *D*-CoO_x-SPL.

The CD spectra of *L*-TA and *D*-TA exhibited absorption onset at 400 nm and opposite CD signals below 400 nm in solution because *L*-TA and *D*-TA selectively absorb circularly polarized light (CPL). The opposite signals beyond 400 nm originated from scattering of the CPL, not from the selective absorption of CPL by TA.[1] On the contrary, *L*-CoO_x-SPL and *D*-CoO_x-SPL exhibited optical onset at a wavelength of 500 nm and CD spectra with opposite signals below 500 nm. Although the CD signals between 400 and 500 nm in *L*-CoO_x-SPL and *D*-CoO_x-SPL are relatively small, possibly due to weak absorption at that wavelength range, the fact that pure *L*-TA and D-TA show CD onsets and absorption onsets at 400 nm indicates that *L*-TA and *D*-TA induce a chiroptical response in CoO_x-SPL and the CD signals track the CoO_x absorption between 400 and 500 nm (the regime beyond absorption of pure *L*-TA and *D*-TA ligands).

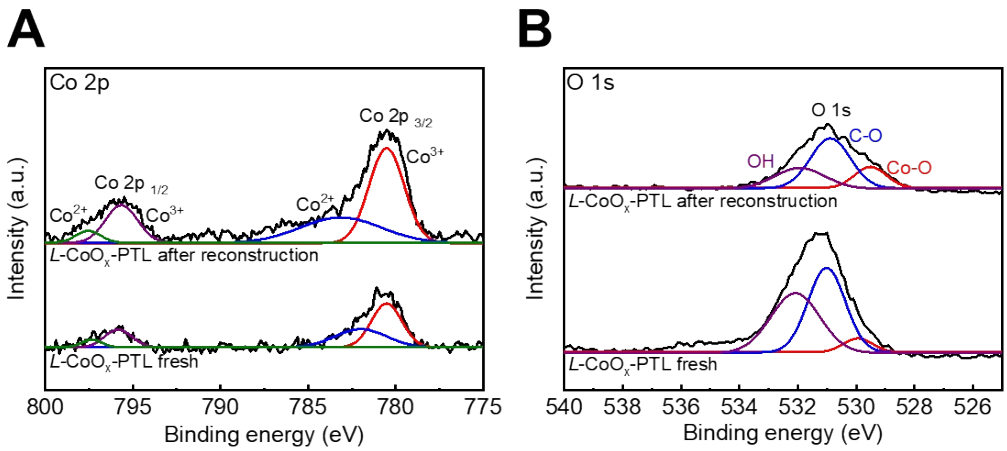

Fig. S8 XPS spectra of Co 2p (A) and O 1s (B) for *L*-CoO_x-PTL fresh and *L*-CoO_x-PTL after reconstruction thin film.

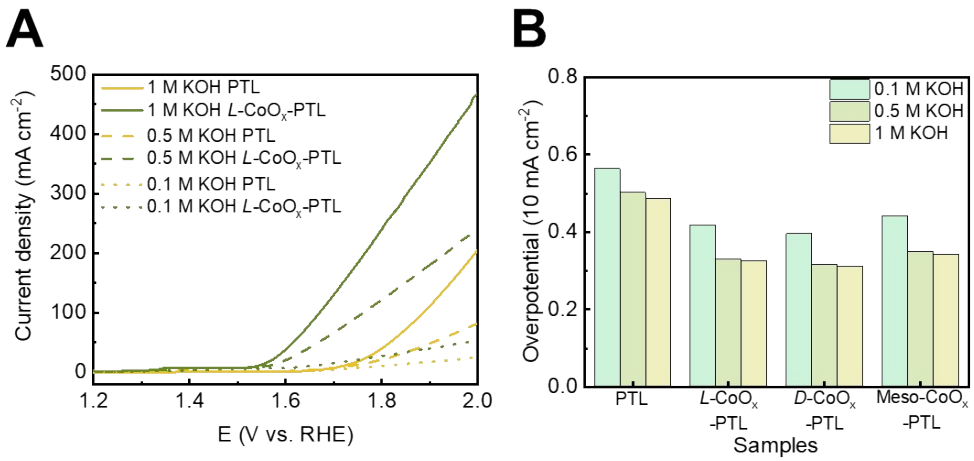

Fig. S9 (A) LSV curves of PTL and *L*-CoO_x-PTL in half-cell oxygen evolution reaction under different KOH concentrations. (B) Comparison of overpotential values of control nickel fiber plate PTL, *L*-CoO_x-PTL, *D*-CoO_x-PTL and *meso*-CoO_x-PTL in half-cell oxygen evolution reaction under different KOH concentrations.

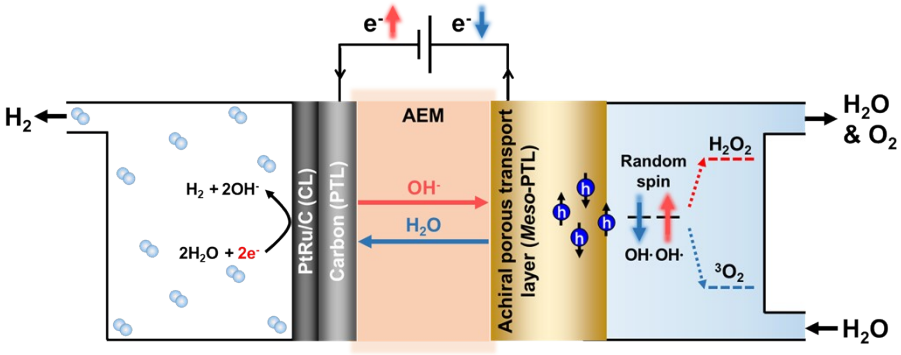

Fig. S10 The mechanism of water electrolysis and electron conductance in spin-unpolarized AEMWE based on *meso*-CoO_x-PTL.

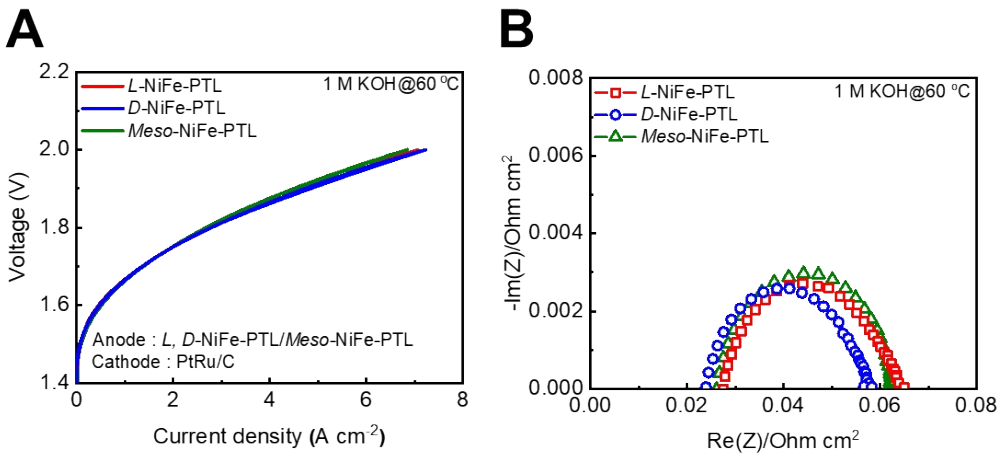

Fig. S11 (A) Polarization curves of AEMWEs based on chiral *L*-NiFe-PTL, *D*-NiFe-PTL and *meso*-NiFe-PTL measured in 1 M KOH at 60℃. (B) EIS Nyquist plots of AEMWEs based on chiral *L*-NiFe-PTL, *D*-NiFe-PTL and *meso*-NiFe-PTL measured in 1 M KOH at 60℃.

Table S1. Summary of the reported properties of AEMWEs in current research

Anode catalyst	Cathode catalyst	Membrane	Electrolyte	Operation temperature (℃)	Current density (A cm^{-2} at V)	Ref.
$CoCrO_x$	Pt/C	PiperION-A60-HCO3	1 M KOH	60	1.5 (2.1)	2
NiFe	NiFe	PFTP-13	1 M KOH	80	1.6 (2)	3
NiFe	PT/C	FAA-3-50	1 M KOH	70	3.6 (1.9)	4
NiFe	Pt/C	QPPBTF-TMA-90	1 M KOH	70	3.4 (2)	5
NiFe	PtRu/C	HTMA-DAPP	1 M NaOH	85	5.3 (1.8)	6
NiFe	PtRu/C	MTCP-50	1M KOH	90	5.4 (1.8)	7
Fe-Ni-Co/HCC	PtRu/C	b-PDTP-Trip-5	1 M NaOH	80	14.17 (2)	8
Fe-Ni-Co/HCC	PtRu/C	Patterned PDTP	1 M NaOH	80	14.47 (2)	9
L-NiFe-PTL	PtRu/C	PDTP-25	1 M KOH	80	11.04 (2)	Our work
D-NiFe-PTL	PtRu/C	PDTP-25	1 M KOH	80	11.5 (2)	Our work
Meso-NiFe-PTL	PtRu/C	PDTP-25	1 M KOH	80	10.83 (2)	Our work

Supplementary References

1. J. Ahn, E. Lee, J. Tan, W. Yang, B. Kim and J. Moon, *Mater. Horiz.*, 2017, **4**, 851-856.
2. S. Li, W. Zhang, M. Wang, H. Zhang, C. Qin, L. Zhang, Y. Chen, S. Jiang, D. Liu, X. Liu, H. Wang, Q. Luo, T. Ding and T. Yao, *Nat. Commun.*, 2024, **15**, 3416.
3. N. Chen, S. Y. Paek, J. Y. Lee, J. H. Park, S. Y. Lee and Y. M. Lee, *Energy Environ. Sci.*, 2021, **14**, 6338-6348.
4. J. E. Park, S. Park, M.-J. Kim, H. Shin, S. Y. Kang, Y.-H. Cho and Y.-E. Sung, *ACS Catal.,* 2022, **12**, 135-145.
5. S. J. Lee, S.-H. Shin, M. S. Cha, S. H. Yang, T. H. Kim, H. J. Cho, K.-H. Oh, T.-H. Kim, S. Kim and J. Y. Lee, *Mater. Today Energy*, 2024, **43**, 101602.
6. D. Li, E. J. Park, W. Zhu, Q. Shi, Y. Zhou, H. Tian, Y. Lin, A. Serov, B. Zulevi, E. D. Baca, C. Fujimoto, H. T. Chung and Y. S. Kim, *Nat. Energy*, 2020, **5**, 378-385.
7. W. Song, K. Peng, W. Xu, X. Liu, H. Zhang, X. Liang, B. Ye, H. Zhang, Z. Yang, L. We, X. Ge and T. Xu, *Nat. Commun.*, 2023, **14**, 2732.
8. C. Hu, N. Y. Kang, H. W. Kang, J. Y. Lee, X. Zhang, Y. J. Lee, S. W. Jung, J. H. Park, M.-G. Kim, S. J. Yoo, S. Y. Lee, C. H. Park and Y. M. Lee, *Angew. Chem. Int. Ed.,* 2024, **63**, e202316697.
9. C. Hu, Y. J. Lee, Y. Ma, X. Zhang, S. W. Jung, H. Hwang, H. K. Cho, M.-G. Kim, S. J. Yoo, Q. Zhang and Y. M. Lee, *ACS Energy Lett.*, 2024, **9**, 1219-1227.